J Therm Spray Tech (2023) 32:1108–1114
https://doi.org/10.1007/s11666-022-01516-8

PEER REVIEWED

Deposition, Microstructure and Thermal Cycling Performance of Strain-Tolerant Thermal Barrier Coatings

Dianying Chen[1] · Christopher Dambra[1] · Mitchell Dorfman[1]

Submitted: 15 July 2022 / in revised form: 5 December 2022 / Accepted: 5 December 2022 / Published online: 19 December 2022

Abstract Thermal barrier coatings (TBCs) with high thermal strain tolerance and erosion resistance are strongly desired in gas turbine engines. Air plasma-sprayed (APS) strain-tolerant dense vertically cracked (DVC) TBCs are now one of the standards used for components of gas turbines. The APS DVC TBCs microstructure is typically achieved utilizing high enthalpy plasma conditions at short standoff distance ($\sim$ 60 mm) in order to achieve larger tensile stress for vertical crack formation. However, shorter standoff distances bring new challenges and are not practical when coating the large and complex geometries of blades and vanes since the plasma torch may collide with the component during spraying. Therefore, there is a need to develop DVC TBCs at longer standoff distances. In this work, dense and strain-tolerant yttria stabilized zirconia thermal barrier coatings exhibiting various vertical crack densities were developed using the high enthalpy TriplexPro plasma torch at spray distances $\geq$ 100 mm. The relationships among spray distances, particle in-flight states, deposition temperatures and coating microstructures were investigated. With the increase in spray distance, both the particle temperatures and vertical crack densities decrease. Coatings with vertical crack densities $\sim$ 3.2 cracks/mm and $\sim$ 1.2 cracks/mm were successfully made at standoff distances 100 mm and 150 mm, respectively. The effect of vertical crack densities on coating durability was evaluated in furnace cycling testing (FCT) and burner rig thermal shock testing. Coatings with higher vertical crack densities showed longer thermal cycling lives in both the FCT and burner rig test.

✉ Dianying Chen
dianying.chen@oerlikon.com

[1] Oerlikon Metco (US) Inc., Westbury, NY, USA

Keywords burner rig test · dense vertically cracked (DVC) · furnace cycle test · thermal barrier coatings · triplexPro-210

Introduction

Thermal barrier coatings have been widely used to decrease the temperature of metallic components in hot sections of turbines used in the aerospace and power generation industries. Yttria stabilized zirconia (YSZ) is one of the most widely used coatings for thermal barrier applications due to its low thermal conductivity, relatively high coefficient of thermal expansion (CTE) and high temperature capability (Ref 1, 2). Air plasma spray (APS) and electron-beam physical-vapor deposition (EB-PVD) are the most widely used deposition processes for the fabrication of YSZ TBCs (Ref 1–4). APS is a relatively lower cost process with higher deposition rates and wider composition flexibility than the EB-PVD process. A typical APS coating has a highly defective microstructure containing microcracks, splat boundaries and $\sim$ 5–20% voids; these microstructural features are desired to lower the thermal conductivity of TBCs and thus reduce heat flux transfer to the metallic bond coat and components. In contrast, EB-PVD TBCs consist of a fine columnar microstructure that provides a much higher degree of strain accommodation for the coefficient of thermal expansion mismatch between the metallic substrate and the ceramic top coat. Generally, EB-PVD TBCs have superior thermomechanical cycling durability over APS TBCs due to their unique strain-tolerant columnar microstructures. However, the relatively high cost of the EB-PVD process limits its application only to highly stressed airfoils in aero engines. In contrast, APS

YSZ TBCs are the choice for combustion liners and blades and vanes of industrial gas turbines (IGT).

The highly durable EB-PVD TBCs with strain-tolerant columnar microstructures drive the design and development of segmented TBCs using the relatively low-cost plasma spray process (Ref 5-10). Dense vertically cracked (DVC) TBCs using the APS process have been developed and successfully implemented in the hot sections of aero and industrial gas turbine engines (Ref 2, 3, 7, 11). Guo et al. (Ref 9) investigated the effect of powder morphology and deposition temperature on APS coating microstructure and deposited the TBC with vertical crack densities of 3.7 cracks/mm at standoff distance of 60 mm. With optimized plasma spraying conditions, segmented thermal barrier coatings with a thickness of 500 μm and vertical crack densities above 8.0 cracks/mm were successfully produced by Karger et al. at standoff distance of 80 mm using a Triplex plasma torch (Ref 8). The high crack density coating showed an improved performance in thermal cycling tests compared to the low crack density coatings (Ref 8). A good thermal shock-resistant TBC typically contains 0.8–8.0 vertical cracks per millimeter (Ref 12). The high in-plane compliance DVC TBC microstructure allows greater TBC layer thickness to have better thermal cycling resistance than conventional low density YSZ coatings (Ref 12). In order to achieve larger tensile stress for vertical crack formation, hot plasma spraying conditions (Ref 13) and short standoff distances ($\sim$ 60 mm) are normally required. However, shorter standoff distances bring new challenges and are not practical when coating the large and complex geometries of IGT blades and vanes since the plasma torch may collide with the component during spraying. Therefore, it is essential to develop segmented DVC TBCs at longer standoff distances to simplify the plasma torch manipulation and robotic programming for spraying complex components. In past decades, both high-power and cascaded plasma torches, such as the TriplexPro-210 and Plazjet, have been developed. This work will focus on the triple-cathode, cascaded plasma torch which features a stable and well-defined arc behavior that results in extremely uniform powder heating and significant improvements in gun performance (Ref 14). The stable and much longer plasma jet of the TriplexPro-210 enables the fabrication of segmented TBCs at relatively long standoff distances.

Even though segmented TBCs have been widely applied in gas turbine engines, the effects of segmented crack density on coating durability have not been systematically studied. The objective of this work is to develop segmented DVC TBCs at longer standoff distance ($\geq$ 100 mm) and to evaluate the effects of vertical crack density on the TBC durability under isothermal and temperature gradient thermal cycling conditions.

Experimental

Metco 204F HOSPed powder (Oerlikon Metco, NY, USA) with a particle size of $-45/+15$ μm was used for the coating deposition. The coatings were sprayed using the TriplexPro-210 plasma gun with argon and hydrogen as the primary and the secondary plasma gases, respectively. The detailed experiments are shown in Table 1. Three sets of coatings were deposited using 85 KW plasma power at standoff distances of 100 mm, 125 mm and 150 mm, while the remaining processing parameters were kept constant. All coatings were deposited onto ϕ25.4 mm $\times$ 6 mm Hastelloy substrates with an Amdry 995C (CoNiCrAlY) bond coat. For all of the coatings sprayed, single-pass plasma torch preheating over the substrate surface was performed to remove surface moisture. During the coating run, K-type thermocouples were attached to the substrate backside to record the deposition temperature. For thermal cycling samples, each TBC system consisted of a $\sim$ 150 μm thick bond coat and a $\sim$ 1000 μm thick top coat. A non-segmented porous TBC using the same Metco 204F powder was also deposited onto the same type of Amdry 995C coated Hastelloy substrate using the TriplexPro-210 torch in order to compare the properties with the segmented DVC TBCs.

In-flight particle diagnostics were conducted to measure the particle temperature (T) and velocity (V) using a DPV-2000 system (Tecnar Automation Ltd., Quebec, Canada). The values of T and V were measured at the center of the particle flux for 3000 particles.

The coating microstructures were characterized using a scanning electron microscope (Hitachi S-3400 N, Hitachi America, Ltd.). The density of vertical cracks (cracks running perpendicular to the coating surface and penetrating at least 1/2 of the coating thickness) was calculated by dividing the number of vertical cracks in the horizontal length of the polished coating cross section.

Vickers microhardness (HV300g) was measured on the polished coating cross sections. The hardness value reported for each sample is the average of 10 measurements. The erosion resistance of coatings was measured using an erosion test rig according to the ASTM G76 specification. In the erosion test, Al_2O_3 powder with particle sizes of 40–80 μm was used as the erodent. It was accelerated at room temperature onto the coating surface at an angle of 20° until a specific dose of approximately 600 g had been delivered. The depth of the eroded crater was then measured. The erosion resistance is expressed in seconds/μm. The reported erosion resistance value is the average of measurements on three coating samples for each system.

Both furnace cycling tests (FCT) and burner rig thermal shock tests were performed for the evaluation of coating

Table 1 Process conditions and Metco 204F YSZ coating results

Coating ID	Plasma power, kW	Standoff (SD) distance, mm	T, °C	V, m/s	Deposition temperature, °C	Vertical crack density (#of cracks/mm)
A	85	100	3680 ± 164	331 ± 45	~ 718	~ 3.2 ± 0.12
B	85	125	3616 ± 161	327 ± 52	~ 647	~ 2.3 ± 0.09
C	85	150	3586 ± 159	322 ± 65	~ 580	~ 1.2 ± 0.08

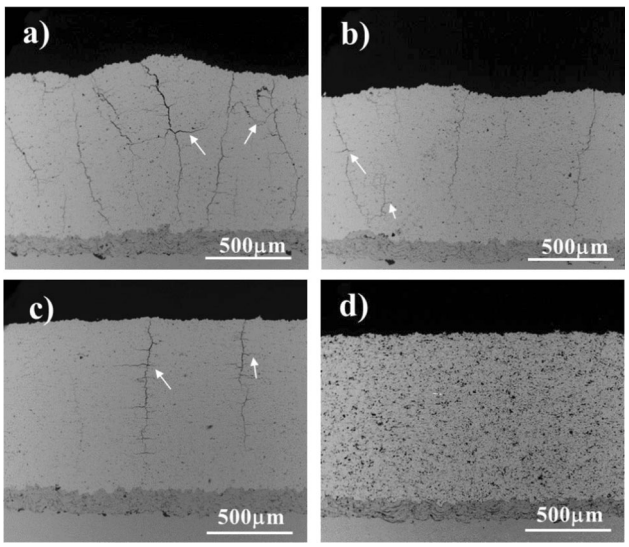

Fig. 1 Metco 204F coating cross section microstructures. (a) Coating A, 100 mm SD; (b) Coating B, 125 mm SD; (c) Coating C, 150 mm SD; (d) non-segmented YSZ TBC

durability. Furnace cycling tests (FCT) were carried out using a CM^{TM} rapid temperature furnace (CM Bloomfield, N.J.). The one-hour thermal cycle consisted of a 10-min heat-up from room temperature to 1125 °C, a 40-min hold at 1125 °C and a 10-min forced air quench. A total of three TBC samples were cycled for each system. The coating was considered to be at failure when spallation was observed. Burner rig thermal shock testing was performed in a gas burner test apparatus operating with propane gas and oxygen. The testing was for 7000 cycles at surface temperature of 1550 °C, followed by 1000 cycles at 1750 °C surface temperature. Ramp-up was 20 s followed by 20 s air cool-down. The back side temperature was maintained at ~ 955 °C. The temperatures were measured using an infrared pyrometer. The lifetime of the coating was defined as the number of thermal cycles at which spallation of the coating can be visibly observed. The rapid heating and cooling cycles ensured the temperature gradients present both radially and through the thickness of the test coupons.

Results and Discussion

In-flight Particle States and Coating Deposition Temperature

The average temperature and velocity of particles in-flight are summarized in Table 1. Both particle temperature and velocity decreased with the increase in standoff distance. The average particle temperature dropped from 3680 °C at 100 mm standoff distance (Coating A) to 3586 °C at 150 mm standoff distance (Coating C). At the same time, the average particle velocity dropped from 331 m/s at 100 mm standoff distance to 322 m/s at 150 mm standoff distance. In all the three process conditions, the average particle temperatures were much higher than the melting temperature of 8YSZ (~ 2700 °C). Therefore, most of the particles will experience overheating and fully melt in the plasma jet even at a longer standoff distance of 150 mm.

The backside substrate temperatures measured during coating deposition were recorded and shown in Table 1. The substrate temperature at 100 mm standoff distance was ~ 718 °C and it decreased to ~ 647 °C at standoff distance of 125 mm and then further decreased to ~ 580 °C at standoff distance of 150 mm. The decrease in deposition temperature with increase in standoff distance can be attributed to the reduced heat transfer from impacting particles and the plasma jet to the substrate. Due to the decrease in deposition temperature, it can be inferred that the thermal stress during coating deposition will decrease with the increase in standoff distance.

Microstructure of As-Deposited TBCs

Figure 1a-C shows the coating cross section microstructures at various standoff distances. All coatings exhibited dense vertically cracked (DVC) microstructures with porosities < 3% and a thickness of approximately 1000 µm. Most of the vertical cracks propagated through the entire coating thickness. The coating vertical crack densities were measured and are summarized in Table 1. At 100 mm standoff distance, the coating had a vertical crack density of ~ 3.2 cracks/mm and decreased to ~ 2.3 cracks/mm at 125 mm standoff distance, and then further

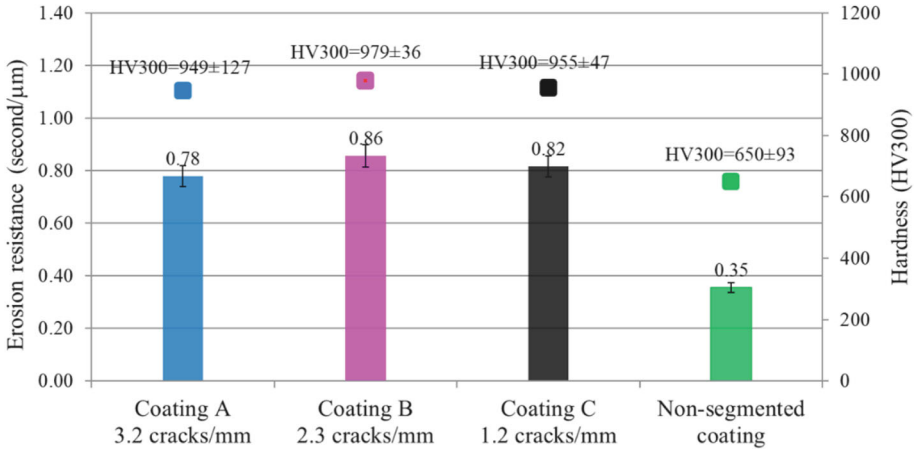

Fig. 2 Coating hardness and erosion resistance. (Scatters represent the hardness value and columns represent the erosion resistance data)

decreased to ~ 1.2 cracks/mm at 150 mm standoff distance. Standoff distance had a significant effect on coating vertical crack density. Closer standoff distance is favorable for producing coatings with higher vertical crack densities. In some local regions, some short horizontal cracks stemming from the vertical cracks are also observed in all the three DVC TBCs (Arrows indicated in Fig. 1). These horizontal cracks are probably caused by the non-uniform distribution of temperature and stress in localized regions. The results demonstrated that segmented DVC TBCs with various crack densities can be produced at longer standoff distances using the cascaded TriplexPro-210 plasma torch. As a reference, the non-segmented YSZ TBC with ~ 8% porosity and 1000 μm thickness is shown in Fig. 1d. The non-segmented TBC used here is for performance comparison only with the segmented TBCs and does not represent the industry standard.

Formation of vertical cracks in the APS TBCs is generally related to the in-plane tensile stresses induced by the thermal expansion coefficient mismatch between coating and substrate as well as the transitional cooling during the coating deposition (Ref 15). The coating deposition temperature and the average temperature of the impacting particles are the two major factors affecting the stress levels. In the present experiments, both the particle temperature and deposition temperature decreased with the increase in standoff distance as shown in Table 1; therefore, coating tensile stress will decrease with the increase in standoff distance. As a result, coating vertical crack density decreased.

Solid Particle Erosion Resistance

In gas turbine engine environments, solid particles could be ingested into the turbine, erode the coating gradually and cause the superalloy substrate to be exposed to temperatures higher than expected (Ref 16, 17). Therefore, coatings with higher erosion resistance are desired. Solid particle erosion resistance for the segmented DVC TBCs and the non-segmented TBCs are shown in Fig. 2. The erosion resistance represents the time needed to erode 1 μm of coating thickness and is expressed as second/μm. A higher erosion resistance value means superior erosion resistance. The dense segmented DVC coatings had erosion resistance values ranging from 0.78 s/μm to 0.86 s/μm. The non-segmented porous coating had an erosion resistance value of 0.35 s/μm. The erosion resistance of the segmented DVC coatings were over two times as high as the porous reference coating. Vickers microhardness measurements showed that all of the segmented DVC TBCs had Vickers hardnesses of HV300 = ~ 950 and the non-segmented porous reference TBC had a Vickers hardness of HV300 = ~ 650. This clearly demonstrates that denser and harder coatings are more erosion resistant.

Furnace Cycling Test (FCT)

The thermal cycle lives of the segmented and non-segmented reference coatings are plotted in Fig. 3. All of the segmented DVC coatings outperformed the reference TBCs in furnace cyclic tests. The non-segmented TBCs had an average life of 40 cycles and the average lives of segmented DVC TBCs ranged from 90 to 500 cycles depending on the vertical crack densities. The cycle lives increased with the increase in coating vertical crack densities.

It was observed that all of the samples failed by delamination of the entire ceramic top coat from the substrate near the bond coat interface. For the FCT failed samples, polished cross sections were examined. The typical microstructures of the failed TBCs are shown in Fig. 4. It was observed that a thin TGO layer was formed on the bond coat surface in all of the failed samples and that the failures of all coatings occurred at the YSZ/TGO interface.

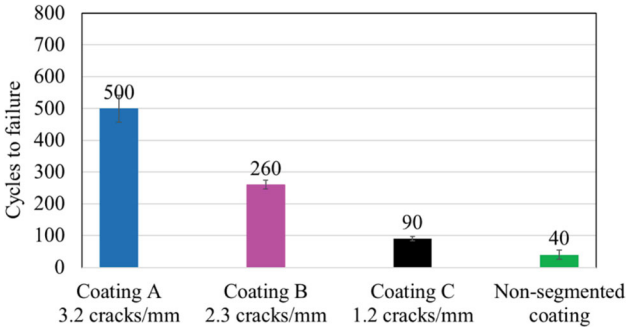

Fig. 3 Furnace thermal cycling lives of dense segmented and the reference non-segmented TBCs

Views under high magnification show the typical TGO morphology in the failed sample (Fig. 5). The TGO was composed of two distinguished phases with dark and gray colors. Energy-dispersive x-ray spectroscopy analysis confirmed the dark-color phase was composed of Al_2O_3 and the gray color phase was mainly composed of Co, Ni, Cr-rich mixed oxides. The formation of these oxides was the result of depletion of Al in the bond coat.

The failure of plasma-sprayed TBCs under furnace cycling had been widely investigated in past studies (Ref 18–20). It is generally agreed that the predominant TBC failure mechanisms are (Ref 1) Stresses induced by metal-ceramic coefficient of thermal expansion (CTE) mismatch and (Ref 2) formation of the thermally growth oxides (TGO) as a result of oxidation of the bond coat. Growth of the oxide scale will induce interfacial volume increases between top coat and bond coat and thus generated stress on the TBCs system. In this study, with the same type of bond coat and test conditions, the oxidation and TGO growth rates for all of the TBC systems should not be significantly different. TGO growth itself cannot explain the relatively quick failure of the non-segmented TBCs as well as the TBCs with low vertical crack densities. Therefore, the degree of strain tolerance in the top coat microstructures played a significant role for TBC durability. It is very crucial to develop a TBC with a higher thermal strain-tolerant microstructure for a longer service life.

Burner Rig Cycle Test

The results for the burner rig thermal shock tests are summarized in Table 2 and the coating appearances are shown in Fig. 6. The non-segmented reference coating failed completely after ~ 1850 cycling test (Fig. 6d) and, in contrast, all of the segmented DVC TBCs survived 7000 cycles at 1550 °C surface temperature with no observed failures. To accelerate coating failure, burner rig tests with increased temperature gradient were further performed. The test included 1000 cycles at surface temperature of 1750 °C following the 7000 cycles at 1550 °C on the

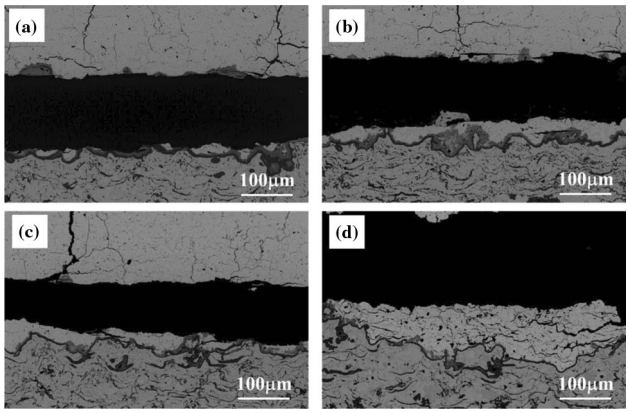

Fig. 4 SEM cross-sectional microstructures of failed TBCs. (a) Coating A after 560 FCT cycles; (b) Coating B after 260 FCT cycles; (c) Coating C after 100 FCT cycles; (d) reference non-segmented porous TBCs after 60 FCT cycles

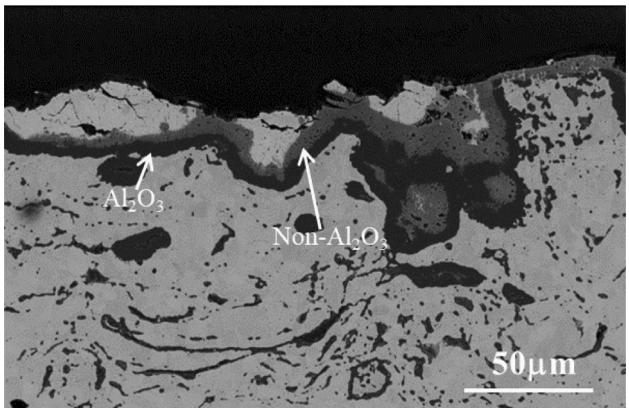

Fig. 5 SEM microstructure showing the typical TGO morphology in the failed TBCs. (coating A after 560 FCT cycles)

segmented DVC TBCs. After 8000 total cycling tests, only Coating A survived and all other segmented DVC coatings failed with various degree of top coat spallation (Fig. 6a-c). It was observed that Coating B exhibited ~ 50% spallation failure, and ~ 90% spallation failure for Coating C. The top coat spallation area increased with the decrease of vertical crack densities.

The coating cross-sectional microstructures for Coating A after 8000 burner rig cycles is shown in Fig. 7. The DVC top coat still adhered very well to the bond coat. A very thin TGO layer can be seen at the interface between bond coat and top coat. In addition, oxidation within the bond coat was also observed along the inter-splat boundaries. Due to the relatively lower temperature by back side cooling during burner rig testing, the TGO growth in bond coat was not as severe as that in the FCT test.

The superior durability of the segmented DVC coatings relative to the non-segmented reference coatings in both

Table 2 Summary on the burner rig test results

Coatings	1850 cycles at 1550 °C	7000 cycles at 1550 °C	7000 cycles at 1550 °C + 1000 cycles at 1750 °C
A	PASS	PASS	PASS
B	PASS	PASS	~ 50% FAIL
C	PASS	PASS	~ 90% FAIL
Reference non-segmented TBCs	100% FAIL	…	…

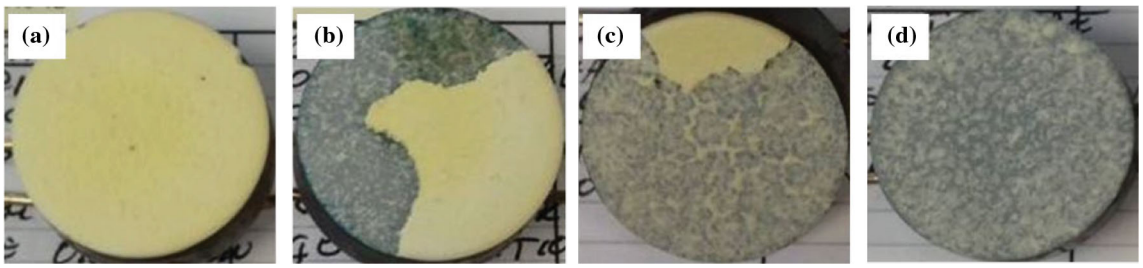

Fig. 6 Coating appearance after burner rig cycling test. (a) coating A after 8000 cycles showing no spallation; (b) Coating B after 8000 cycles showing ~ 50% coating spallation; (c) Coating C after 8000 cycles showing ~ 90% coating spallation; (d) Non-segmented reference coating showing 100% spallation after 1850 cycles at 1550 °C surface temperature

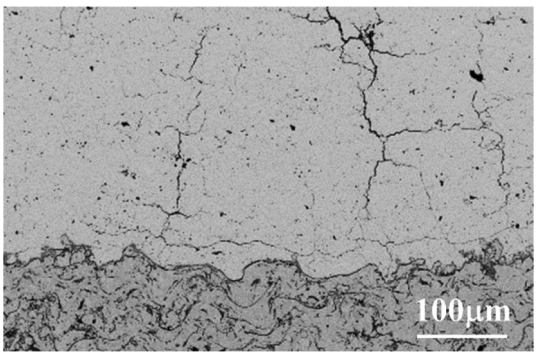

Fig. 7 Cross-sectional microstructure of coating A after 8000 burner rig thermal cycles

the furnace cycle testing and burner rig testing can be attributed to their improved strain tolerance. The higher the amount of vertical cracks, the higher the coating strain tolerance. Therefore, TBCs with a high vertical crack density exhibited a significant improvement in their thermal cycle life compared to the TBCs with low segmentation crack density or non-segmented TBCs. The coating with the highest crack density performed the best.

Conclusions

Deposition of dense vertically cracked (DVC) yttria stabilized zirconia thermal barrier coatings at standoff distances $\geq$ 100 mm was successfully developed and demonstrated using the cascaded TriplexPro-210 plasma torch. Standoff distance had a great effect on coating vertical crack densities. Both furnace cycling tests and burner rig thermal shock tests indicated that TBCs with a higher vertical crack density exhibited a significant improvement in their thermal cycle life compared to the TBCs with low vertical crack density or non-segmented TBCs. In addition, the erosion resistance of DVC TBCs were over two times as high as the reference non-segmented porous coatings. The TriplexPro-210 plasma torch demonstrated to be a very effective tool in producing erosion-resistant and durable strain-tolerant TBCs at longer standoff distances.

References

1. N.P. Padture, M. Gell and E.H. Jordan, Thermal Barrier Coatings for Gas-Turbine Engine Applications, *Science*, 2002, **296**, p 280-284.
2. R.A. Miller, Thermal Barrier Coatings for Aircraft Engines: History and Directions, *J. Therm. Spray Technol*, 1997, **6**, p 35-42.
3. A. Feuerstein, J. Knapp, T. Taylor, A. Ashary, A. Bolcavage and N. Hitchman, Technical and Economical Aspects of Current Thermal Barrier Coating Systems for Gas Turbine Engines by Thermal Spray and EBPVD: A Review, *J. Therm. Spray Technol*, 2008, **17**, p 199-213.
4. R. Darolia, Thermal Barrier Coatings Technology: Critical Review, Progress Update, Remaining Challenges and Prospects, *Int. Mater. Rev.*, 2013, **58**, p 315-348.
5. D. Chen, C. Dambra and M. Dorfman, Process and Properties of Dense and Porous Vertically-Cracked Yttria Stabilized Zirconia

Thermal Barrier Coatings, *Surf. Coat. Technol.*, 2020, **404**, p 126467.
6. D. Chen, R. Rocchio-Heller and C. Dambra, Segmented Thermal Barrier Coatings for ID and OD Components Using the SinplexPro Plasma Torch, *J Therm Spray Tech*, 2019, **28**, p 1664-1673.
7. T. A. Taylor, Thermal barrier coating for substrates and process for producing it. (1991) US Patent No. 5073433.
8. M. Karger, R. Vaßen and D. Stöver, Atmospheric Plasma Sprayed Thermal Barrier Coatings with High Segmentation Crack Densities: Spraying Process, Microstructure and Thermal Cycling Behavior, *Surf. Coat. Technol.*, 2011, **206**, p 16-23.
9. H.B. Guo, S. Kuroda and H. Murakami, Segmented Thermal Barrier Coatings Produced by Atmospheric Plasma Spraying Hollow Powders, *Thin Solid Films*, 2006, **506–507**, p 136-139.
10. I. E. Sumner, & D. L. Ruckle, Development of improved-durability plasma sprayed ceramic coatings for gas turbine engines, in AIA/SAE/ASME 16th Joint Propulsion Conference, pp. 1193 (1980).
11. C.U. Hardwicke and Y.C. Lau, Advances in Thermal Spray Coatings for Gas Turbines and Energy Generation: A Review, *J Therm Spray Tech*, 2013, **22**, p 564-576.
12. T. A. Taylor, Dense Vertically Segmented Thermally Sprayed YSZ for TBC and other High Temperature Applications, in Proceedings of the 22nd Heat Treating Society Conference and the 2nd International Surface Engineering Congress, pp. 539-548 (2003).
13. R. Vaßen, E. Bakan, D. Mack et al., A Perspective on Thermally Sprayed Thermal Barrier Coatings: Current Status and Trends, *J Therm Spray Tech.*, 2022, **31**, p 685-698.
14. D. Hawley, Improved Quality, Reduced Cost and Cycle Times, *Sulzer Tech. Rev.*, 2007, **3**, p 14-16.
15. L. Xie, D. Chen, E. Jordan, A. Ozturk, F. Wu, X. Ma, B. Cetegen and M. Gell, Formation of Vertical Cracks in Solution-Precursor Plasma-Sprayed Thermal Barrier Coatings, *Surf. Coat. Technol.*, 2006, **201**, p 1058-1064.
16. R.G. Wellman and J.R. Nicholls, A Review of the Erosion of Thermal Barrier Coatings, *J. Phys. D Appl. Phys.*, 2007, **40**, p R293.
17. F. Cernuschi, L. Lorenzoni, S. Capelli, C. Guardamagna, M. Karger, R. Vaßen, K. von Niessen, N. Markocsand, J. Menuey and C. Giolli, Solid Particle Erosion of Thermal Spray and Physical Vapour Deposition Thermal Barrier Coatings, *Wear*, 2011, **271**, p 2909-2918.
18. E.A.G. Shillington and D.R. Clarke, Spalling Failure of a Thermal Barrier Coating Associated with Aluminum Depletion in the Bond-Coat, *Acta Mater*, 1999, **47**, p 1297-1305.
19. A. Rabiei and A.G. Evans, Failure Mechanisms Associated with the Thermally Grown oxide in Plasma-Sprayed Thermal Barrier Coatings, *Acta Mater*, 2000, **48**, p 3963-3976.
20. J.A. Haynes, M.K. Ferber and W.D. Porter, Thermal Cycling Behavior of Plasma-Sprayed Thermal Barrier Coatings with Various MCrAIX Bond Coats, *J. Therm. Spray Technol*, 2000, **9**, p 38-48.